



Cite this: *Nanoscale*, 2018, **10**, 9602

Electrically driven lasers from van der Waals heterostructures

Xun Yang,^{a,b} Chong-Xin Shan,^{a,b} Pei-Nan Ni,^c Ming-Ming Jiang,^a An-Qi Chen,^d Hai Zhu,^d Jin-Hao Zang,^b Ying-Jie Lu^b and De-Zhen Shen^{*a}

Van der Waals heterostructures (vdWHs) have opened new avenues for fundamental scientific studies and design of novel devices. Although numerous reports have demonstrated vdWH optoelectronic devices, no report on vdWH lasers can be found to date. In this paper we demonstrated electrically driven vdWH lasers for the first time, and the lasers were realized from ZnO microwire/MgO/*p*-GaN structures. By coating Ag films on the top surfaces of the ZnO microwires, the current injection and lasing directionality of the vdWH lasers have been improved significantly, and this improvement can be attributed to the high conductivity and reflectivity of the Ag film. The output power of the device can reach 2.41 μ W under 14 mA drive current, which is among the highest values ever reported for ZnO based lasers. Our results may provide a promising way to electrically pumped lasers based on micro/nano-structures.

Received 5th February 2018,
Accepted 16th April 2018

DOI: 10.1039/c8nr01037d

rsc.li/nanoscale

Introduction

Electronic and optoelectronic devices based on van der Waals heterostructures (vdWHs) have attracted significant attention due to their excellent properties.^{1,2} Unlike conventional heterostructures, materials with vdWHs are bonded with each other by van der Waals interaction.^{3–9} Traditional epitaxial growth usually requires small lattice mismatch and elaborate control over growth parameters. However, in vdWHs, it is convenient to construct diverse devices by simply combining low dimensional (1D, 0D or 2D) materials with lattice mismatched materials.^{10–14} The vdWHs therefore provide another choice for functional device design. For instance, vdWHs with varying functionalities, such as photodetectors,^{15–17} photovoltaics,^{18–20} light emitting devices^{21–23} and logic devices,^{24–26} have been reported in recent years. These vdWHs demonstrate unique properties compared with conventional devices. Yet to date, no report on vdWH lasers can be found, which will significantly promote the constructional design of lasers based on low dimensional materials and open another application area for vdWHs.

1D materials such as micro/nanowires have become desirable candidates for laser diodes (LDs), due to their passive waveguides and strong confinement of electrons, holes and photons.^{27–30} In addition, the natural optical cavities and high optical quality of the micro/nano-structures also benefit the miniaturization of semiconductor lasers, which is one of the key elements for on-chip integration of nanophotonics and nanoelectronics, while electrically pumped lasers based on these naturally formed micro/nano-structures have been rarely reported, due to the lack of an effective p–n junction construction method. Coupling the vdWH architectures to 1D materials will lead to more valuable light sources, namely electrically pumped vdWH micro/nano-lasers.

Here in this paper, we demonstrated for the first time the realization of electrically pumped lasers from vdWHs, and the vdWHs were formed from ZnO microwire/MgO/*p*-GaN structures. In these structures, the vdWHs were formed by transferring ZnO microwires (MWs) grown on a Si substrate onto a MgO/*p*-GaN template. The smooth surfaces of the ZnO MW and the *p*-GaN ensure intimate contact, allowing the formation of a vdWH. The ZnO MWs were employed as the active material for the lasers by utilizing their much higher exciton binding energy (60 meV) than the activation energy at room temperature (\sim 25 meV), which ensures that efficient excitonic lasing may be realized *via* the exciton–exciton scattering mode.^{31–40} *p*-GaN was employed as the hole source for the ZnO MWs, and the MgO layer was used to modulate the carrier transportation between the *p*-GaN and ZnO MWs to ensure that the radiative recombination between electrons and holes occurred in the ZnO MWs.^{38,41} Additionally, the ZnO MWs possess six smooth facets, which can serve as a natural whis-

^aState Key Laboratory of Luminescence and Applications, Changchun Institute of Optics, Fine Mechanics and Physics, Chinese Academy of Sciences, Changchun 130033, China. E-mail: shancx@ciomp.ac.cn, shendz@ciomp.ac.cn

^bSchool of Physics and Engineering, Zhengzhou University, Zhengzhou 450052, China

^cCRHEA-CNRS, rue Bernard Grégory, 06560 Valbonne, France

^dState Key Laboratory of Optoelectronic Materials and Technologies, School of Physics, Sun Yat-Sen University, Guangzhou 510275, China

pering-gallery-mode (WGM) micro-cavity for the lasers.^{42–44} Under the injection of a continuous current, electrically pumped lasing has been achieved from the vdWHs. In order to improve the contact between the electrode and the ZnO MWs and the emission directionality of the devices, an Ag film was coated on the ZnO MWs in order to utilize its high conductivity and reflectivity. The threshold for lasing is 12.5 mA, and the output power can reach 2.41 μW when the injection current is 14 mA. This is the first report on vdWH lasers to the best of our knowledge, which also provides an effective way to construct electrical lasers based on naturally formed micro/nano-structures.

Experimental

ZnO MW growth and characterization

The ZnO MWs used in this study were grown by vapor-phase transport (VPT) on silicon substrates. A mixture of ZnO and graphite powders with a definite weight ratio of 1 : 1 served as the reactive source. Si (100) substrates were placed on a quartz boat to collect the products. Then the quartz boat was put into a tube furnace for the growth of ZnO MWs. The growth temperature was set at 1000 $^{\circ}\text{C}$, and a constant flow of argon (120 sccm) was introduced into the tube furnace as protecting gas during the growth process. The structural properties of the ZnO MWs were studied by using a Bruker D8 X-ray diffractometer. The morphology of the ZnO MWs was characterized using a Hitachi S4800 field emission scanning electron microscope (SEM). ZnO MWs were excited by using a Q-switch Nd:YAG nanosecond laser (266 nm), and the laser beam was focused using a cylindrical lens perpendicular to the *c*-axis of the MW.

Device fabrication

The schematic diagram of the vdWH is shown in Fig. 2a, and the fabrication process of the heterostructure is presented as follows: the Mg-doped GaN with a carrier concentration of $5.3 \times 10^{17} \text{ cm}^{-3}$ was used as the substrate. A 10 nm MgO layer was grown on the *p*-GaN by molecular beam epitaxy (MBE). Then a metallic Ni/Au layer was deposited on the *p*-GaN, acting as an electrode, using the thermal evaporation system. Then a ZnO MW was transferred onto the MgO/*p*-GaN substrate. After that, an ITO-coated glass was placed on them to form an electrode. Finally, polymethyl methacrylate (PMMA) in acetone solution (10 mg mL^{-1}) was injected between the ITO and MgO/*p*-GaN. The device was dried in an oven at 90 $^{\circ}\text{C}$ for 20 min. After the evaporation of the acetone, PMMA could fix the device, avoiding the relative movement of the ITO electrode. Moreover, PMMA could serve as the insulating layer between the ITO electrode and the MgO/*p*-GaN substrate.

In order to improve the electrode contact and the lasing directionality, another structure was fabricated following a similar design, in which the ZnO MW was coated with an Ag film. A ZnO MW was transferred onto a silicon substrate. And a 100 nm thick Ag film was deposited on the ZnO MW by

thermal evaporation. Then the Ag-coated ZnO MW (ZnO MW@Ag) was transferred onto the MgO/*p*-GaN substrate with the Ag-coated facets upwards. ZnO MW@Ag/MgO/*p*-GaN vdWHs were fabricated through the same process afterwards.

Device measurements

The current–voltage (*I*–*V*) characteristics of the vdWH were studied by using an Agilent B1500A semiconductor device analyzer. The electroluminescence (EL) spectra of the devices were obtained using a Hitachi F4500 spectrometer. The output power of the lasers was recorded by using an OPHIR Nova II power meter. All measurements were carried out at room temperature.

Results and discussion

Fig. 1a shows the X-ray diffraction (XRD) pattern of the ZnO MWs grown on the Si substrate, which indicates the wurtzite structure and high crystal quality of the MWs. The typical SEM images of the as-grown ZnO MWs are shown in Fig. 1b. The ZnO MWs show a perfect hexagonal cross-section and smooth side facets. The smooth side facets ensure the close proximity of the ZnO MW and the GaN layer to form a high quality vdWH. Fig. 1c presents the room temperature photoluminescence (PL) spectra of an individual ZnO MW with a diameter of about 2.3 μm at a different pumping power density. The spectrum at a low pumping power density (1.05 MW per cm^2) shows a near-band-edge (NBE) emission band

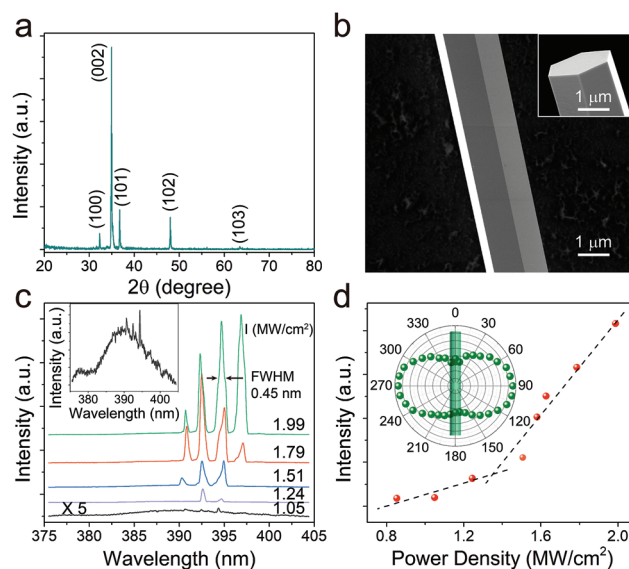


Fig. 1 Characteristics of the ZnO MWs. (a) XRD pattern of the as-grown ZnO MWs. (b) Typical SEM images of the ZnO MWs. The inset shows the end of a ZnO MW. (c) PL spectra of the ZnO MW as a function of pumping power density. Inset, enlarged spectrum at 1.05 MW per cm^2 . (d) Integrated emission intensity of the ZnO MWs versus the pumping power density. The inset shows the plots of lasing emission intensity as a function of the emission polarization angle relative to the microwire axis.

located at 389.6 nm with a series of whispering-gallery-mode (WGM) resonance peaks (inset of Fig. 1c), which derive from the light interference through total internal reflection at the cavity boundary.^{27,43} As the pumping power density is increased to 1.24 MW per cm², these resonance peaks transform into lasing peaks.²⁷ By further increasing the pumping power density, more peaks appear with orders of magnitude higher than the underlying spontaneous emission. The emission intensity of the MWs shows a superlinear dependence on the pumping power intensity (Fig. 1d), indicating the evolution from spontaneous emission to stimulated emission with a threshold of 1.35 MW per cm². The full width at half maximum (FWHM) and mode spacing of the lasing modes are about 0.45 nm and 2.1 nm, respectively. For the lasing peak at 392.3 nm, the corresponding *Q*-factor is estimated to be 872 according to $Q = \lambda/\Delta\lambda$, where $\Delta\lambda$ is the FWHM of the lasing peak.⁴³ The lasing polarization is shown in the inset of Fig. 1d aligned with the ZnO MW. The intensity of polarized emission with the electric field perpendicular to the microwire axis is 2.2 times larger than that parallel to the microwire axis. The polarized emission may be related to the transition selection of the excitons.⁴²

ZnO MW/MgO/*p*-GaN structures were constructed to realize electrically driven lasing from a single ZnO MW, as schematically illustrated in Fig. 2a. The Mg-doped *p*-type GaN was employed as the hole injection layer for the ZnO MW. A 10 nm MgO layer was grown on *p*-GaN by molecular beam epitaxy (MBE) to hinder the electrons in the ZnO MW from entering into the *p*-GaN, thus helping in enhancing the emission from the ZnO MW.^{38,41} Fig. 2b shows the current–voltage (*I*–*V*) curve of the ZnO MW/MgO/*p*-GaN structure, which exhibits the typical rectifying characteristics with a turn-on voltage of 7.8 V. The linear *I*–*V* curves for Ni/Au on *p*-GaN and ITO on ZnO

MWs indicate that good ohmic contacts have been formed. The rectification characteristics indicate the formation of a high quality vdWH between the *p*-GaN and the ZnO MW. The EL spectra of the structure under different injection currents are presented in Fig. 2c. At a low drive current, a broad emission band appears at 385 nm, which can be attributed to the NBE emission of ZnO. The inset shows the emission image of the structure. With increasing the drive current, some sharp peaks with an FWHM of 0.8 nm appear on the shoulder of the broad emission peak, indicating the occurrence of lasing. The dependence of the FWHM and integrated intensity on the injection current is shown in Fig. 2d. The abrupt decrease of the FWHM and the superlinear increase of emission intensity suggest a lasing threshold of 4.8 mA. Note that no report on electrically pumped lasing from vdWHs can be found to date.

Although lasing behaviors have been observed, the performances of the ZnO MW/MgO/*p*-GaN structure are restricted greatly by two factors. On one hand, the resistance of the undoped ZnO MW is as high as 3.7×10^8 ohm cm⁻¹, and the ZnO MW is in contact with the rough ITO glass at discrete points due to the rough surface of the ITO glass, which can also be confirmed from the emission image in the inset of Fig. 2c. It could be clearly seen through naked eyes that the structure could emit brightly at discrete points along the ZnO MW. Thus, the current injection and emission area are severely restricted by the poor electrode contact and high resistance of the ZnO MW. On the other hand, light in the WGM is predominantly emitted out at the corners of the hexagonal cavity, which together with the light leakage at the PMMA/ZnO and ITO/ZnO interfaces lead to poor directionality of the laser.

In order to improve the electrode contact and lasing directionality of the device, ZnO MWs coated with an Ag film (ZnO MW@Ag) were utilized to fabricate vdWH lasers. Fig. 3a shows the schematic diagram of the ZnO MW@Ag/MgO/*p*-GaN structure. To fabricate the ZnO MW@Ag, a single ZnO MW was transferred onto a silicon substrate at first. Then, a 100 nm Ag film was deposited on the ZnO MW through thermal evaporation. Fig. 3b shows the SEM image of the ZnO MW@Ag with a diameter and length of about 1.7 μm and 1.5 cm, respectively. One can see that the three upward facets of the ZnO MW are covered with an Ag film. The inset shows the enlarged SEM image of the surface of the ZnO MW@Ag, from which a continuous Ag film can be observed. Then the ZnO MW@Ag was transferred onto an MgO/*p*-GaN substrate with the Ag covered facets upward to construct the ZnO MW@Ag/MgO/*p*-GaN structure. Fig. 3c shows the *I*–*V* curve of the ZnO MW@Ag/MgO/*p*-GaN structure with a turn-on voltage of 6.4 V. The injection current at the same forward bias is about 6 times higher than the device without an Ag film. The smaller turn-on voltage and larger injection current result from the improved electrode contact by the Ag film. However, the *I*–*V* curve exhibits worse rectifying characteristics compared with that of the device without an Ag film due to the Schottky barrier formed between the ZnO MW and the Ag electrode, which can be confirmed by the *I*–*V* curve of the Ag electrode in contact with the ZnO MW (inset of Fig. 3c). Ag was chosen as the coating metal because

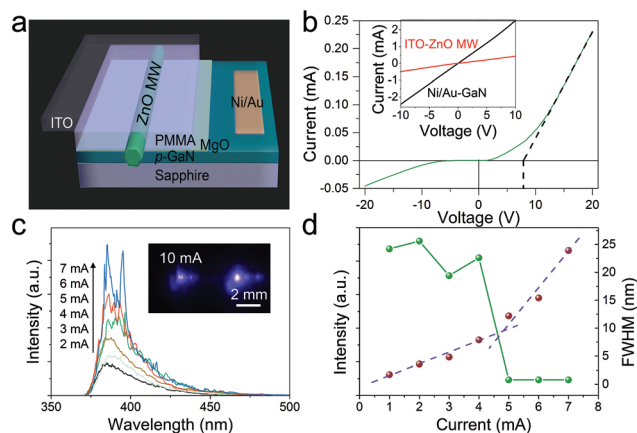


Fig. 2 Schematic diagram and characteristics of the ZnO MW/MgO/*p*-GaN vdWH laser. (a) Schematic diagram of the ZnO MW/MgO/*p*-GaN vdWH laser. (b) *I*–*V* curve of the vdWH. Inset, *I*–*V* curves for Ni/Au on *p*-GaN and ITO on the ZnO MW. (c) EL spectra under different injection currents. The inset shows a typical emission image of the device. (d) Integrated emission intensity and FWHM of the device versus the injection current.

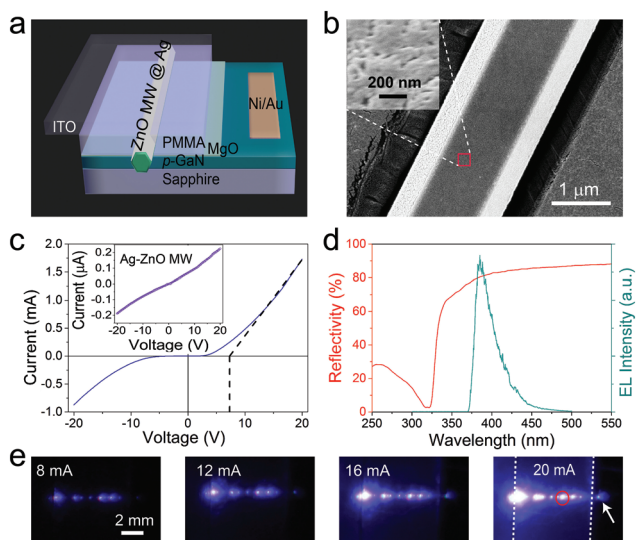


Fig. 3 Schematic diagram and characteristics of the ZnO MW@Ag/MgO/p-GaN vdWH. (a) Schematic diagram of the ZnO MW@Ag/MgO/p-GaN vdWH. (b) SEM image of an individual ZnO MW coated with a 100 nm Ag film. Inset, enlarged surface image of the Ag-coated ZnO MW. (c) I - V characteristics of the vdWH. Inset, the I - V curve of a single ZnO MW with two Ag electrodes 2 mm apart, indicating Schottky contacts between Ag and the ZnO MW. (d) Reflectance spectrum of the Ag film and EL spectrum of the ZnO MW/MgO/p-GaN vdWH. (e) Emission images of the vdWH. The dashed lines in the lower right panel highlight the edge of the GaN film, the arrow highlights the strong emission from the exposed ZnO MW end, and the red circle highlights an emission point.

of its high reflectivity in the near UV region, as shown in Fig. 3d. The Ag film shows a reflectivity above 80% in the emission spectral range of the devices. Thus the Ag film may help us to improve the device emission directionality. The emission images are presented in Fig. 3e. The dashed lines in the right panel highlight the edge of the GaN film, and the arrow highlights the strong emission from the exposed ZnO MW end. The bright emission from the ZnO MW end suggests a strong waveguide behavior of the MW. The emission image of the device without an Ag film shows a few discrete emission points (inset of Fig. 2c), mainly due to the poor contact between the ZnO MW and the ITO glass. Whereas the device with an Ag film shows more emission points along the ZnO MW, which are stable under different drive currents. Additionally, with the increase of the drive current, these emission points grow in brightness and number and turn into short lines. The stable linear emission areas indicate the good stability of the vdWH and the electrode contact, which lay a solid foundation for high performance vdWH lasers.

The influence of the Ag film on the laser output has also been investigated. The optical field distributions in the hexagonal ZnO MW microcavity are simulated using the 2D finite-difference time-domain (FDTD) method. Fig. 4a shows the optical field distribution in a bare ZnO MW. The majority of the light resonates in the hexagonal cavity through total internal reflection at the cavity boundary and is emitted

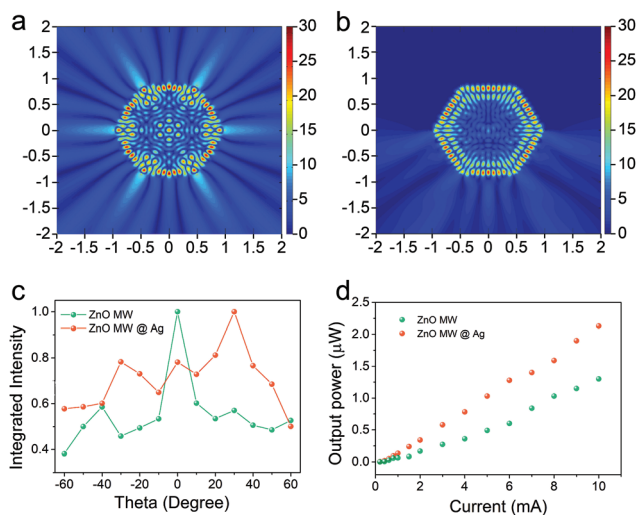


Fig. 4 Emission output modulated by the Ag film. Simulated emission intensity distribution in a 1.7 μm diameter ZnO WGM cavity (a) without an Ag film and (b) with the upper three facets coated with an Ag film with the corresponding resonant wavelength at around 396 nm. (c) Far-field emission intensity distribution around the c -axis of the ZnO MW patterns of devices with and without the Ag film. (d) Output power of the devices with and without the Ag film as a function of the injection current.

mainly from the six corners of the hexagonal structure. When the upward three facets of the ZnO MW are covered with an Ag film, the strong optical loss at the upward corners and facets is prevented significantly due to the high reflectivity of the Ag film, as shown in Fig. 4b. Fig. 4c shows the experimental far-field distribution of the emission intensity measured by rotating the detector around the c -axis of the ZnO MW and theta is defined as the angle between the emission light and the normal of the GaN film. The far-field intensity distribution of both devices with and without the Ag film shows maximum values at around 0° , -30° and $+30^\circ$. The maximum intensity at 0° may come from the reflection between the bottom and top planes. Whereas the maximum values at around -30° and $+30^\circ$ should derive from the WGM resonance in the hexagonal ZnO MW cavity. It is notable that the emission intensity of the device with an Ag film at around -30° and $+30^\circ$ is distinctly enhanced with respect to that of the device without an Ag film, which may be resulted from suppressed light emission at the upward corners and facets (Fig. 4b). Fig. 4d shows the drive current dependent output power of the two devices collected behind the p -GaN. The output power of the device with the Ag film is obviously greater than that of the device without the Ag film, which confirms that the Ag film helps in improving the emission directionality because of its relatively high reflectivity in this region.

The EL spectra of the ZnO MW@Ag/MgO/p-GaN vdWH under different drive currents are presented in Fig. 5a. Under a low injection current, a ZnO NBE emission peak at 385 nm and a series of WGM resonance peaks with an FWHM of 3.4 nm and a spacing of 4.4 nm can be observed, indicating

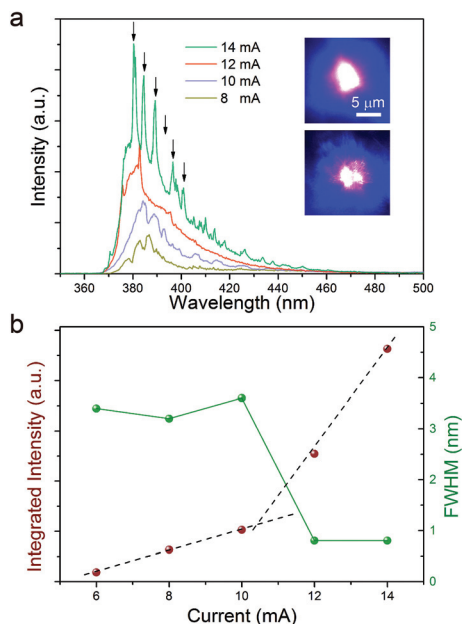


Fig. 5 Lasing characteristics of the ZnO MW@Ag/MgO/p-GaN vdWH laser. (a) EL spectra under different injection currents. The upper and lower panels in the inset show the optical images of the laser at an emission dot of the ZnO MW at an injection current of 10 mA and 16 mA, respectively. (b) Integrated emission intensity and the FWHM of the vdWH laser versus the injection current.

the excellent WGM cavity quality of the ZnO MW. Under an injection current of 12 mA, some quasi-equidistant lasing peaks with the average FWHM as narrow as 0.8 nm emerge. When the injection current is further increased to 14 mA, these lasing peaks grow both in number and intensity. The quasi-equidistant pattern of the lasing peaks shows an average mode spacing of 4.12 nm, as denoted by arrows. The inset of Fig. 5a shows the optical images of the vdWH laser at an emission dot of the ZnO MW, as denoted by the red circle in Fig. 3e, below (10 mA) and above (16 mA) the threshold. A clear interference image can be observed when the injection current is above the threshold, indicating strong spatial coherence. Fig. 5b shows the dependence of the spectral FWHM and integrated spectra intensity of the ZnO MW@Ag/MgO/p-GaN vdWH on the injection current. The abrupt decrease of the FWHM and the superlinear increase of emission intensity evidence a lasing threshold of ~ 12.5 mA. The output power of the device can reach $2.41 \mu\text{W}$ under 14 mA drive current, which is among the highest values ever reported for ZnO based lasers.

Conclusions

In this study, electrically driven lasers have been realized from vdWHs for the first time employing ZnO MWs as a gain medium, and an Ag film was coated on the ZnO MWs to improve the current injection and emission directionality of the vdWH lasers. The laser exhibited a threshold of 12.5 mA,

and the output power could reach $2.41 \mu\text{W}$ at 14 mA. The present work demonstrated the first electrically driven vdWH laser, which may provide a simple route to construct electrically pumped lasers based on naturally formed micro/nanostructures, and may also extend the applications of vdWHs.

Conflicts of interest

There are no conflicts to declare.

Acknowledgements

This work was financially supported by the National Natural Science Foundation of China (U1604263 and 61604132), and the National Science Foundation for Distinguished Young Scholars of China (61425021).

Notes and references

- 1 D. Jariwala, T. J. Marks and M. C. Hersam, *Nat. Mater.*, 2017, **16**, 170.
- 2 D. Jariwala, V. K. Sangwan, L. J. Lauhon, T. J. Marks and M. C. Hersam, *ACS Nano*, 2014, **8**, 1102.
- 3 J. Dong, F. Liu, F. Wang, J. Wang, M. Li, Y. Wen, L. Wang, G. Wang, J. He and C. Jiang, *Nanoscale*, 2017, **9**, 7519–7525.
- 4 Y. Yamasaki, R. Moriya, M. Arai, S. Masubuchi, S. Pyon, T. Tamegai, K. Ueno and T. Machida, *2D Mater.*, 2017, **4**, 041007.
- 5 H. Ko, K. Takei, R. Kapadia, S. Chuang, H. Fang, P. W. Leu, K. Ganapathi, E. Plis, H. S. Kim and S. Y. Chen, *Nature*, 2010, **468**, 286–289.
- 6 B. Wang, S. Yang, C. Wang, M. Wu, L. Huang, Q. Liu and C. Jiang, *Nanoscale*, 2017, **9**, 10733–10740.
- 7 A. S. Sarkar and S. K. Pal, *J. Phys. Chem. C*, 2017, **121**, 21945–21954.
- 8 J. Li, X. Guan, C. Wang, H. C. Cheng, R. Ai, K. Yao, P. Chen, Z. Zhang, X. Duan and X. Duan, *Small*, 2017, **13**, 1701034.
- 9 C. H. Ma, J. C. Lin, H. J. Liu, T. H. Do, Y. M. Zhu, T. D. Ha, Q. Zhan, J. Y. Juang, Q. He and E. Arenholz, *Appl. Phys. Lett.*, 2016, **108**, 253104.
- 10 T. Amrillah, Y. Bitla, K. Shin, T. Yang, Y. H. Hsieh, Y. Y. Chiou, H. J. Liu, T. H. Do, D. Su and Y. C. Chen, *ACS Nano*, 2017, **11**, 6122.
- 11 A. K. Geim and I. V. Grigorieva, *Nature*, 2013, **499**, 419–425.
- 12 M. I. Utama, Q. Zhang, J. Zhang, Y. Yuan, F. J. Belarrie, J. Arbiol and Q. Xiong, *Nanoscale*, 2013, **5**, 3570–3588.
- 13 K. Chung, S. I. Park, H. Baek, J. S. Chung and G. C. Yi, *NPG Asia Mater.*, 2012, **4**, e24.
- 14 M. Yankowitz, J. Xue, D. Cormode, J. D. Sanchezyamagishi, K. Watanabe, T. Taniguchi, P. Jarilloherrero, P. Jacquod and B. J. Leroy, *Nat. Phys.*, 2012, **8**, 382–386.
- 15 F. H. Koppens, T. Mueller, P. Avouris, A. C. Ferrari, M. S. Vitiello and M. Polini, *Nat. Nanotechnol.*, 2014, **9**, 780.

- 16 Z. Sun, Z. Liu, J. Li, G. A. Tai, S. P. Lau and F. Yan, *Adv. Mater.*, 2012, **24**, 5878–5883.
- 17 P. Li, K. Yuan, D. Y. Lin, X. Xu, Y. Wang, Y. Wan, H. Yu, K. Zhang, Y. Ye and L. Dai, *Nanoscale*, 2017, **9**, 18175–18179.
- 18 V. V. Brus, M. A. Gluba, X. Zhang, K. Hinrichs, J. Rappich and N. H. Nickel, *Phys. Status Solidi A*, 2014, **211**, 843–847.
- 19 E. Shi, H. Li, L. Yang, L. Zhang, Z. Li, P. Li, Y. Shang, S. Wu, X. Li and J. Wei, *Nano Lett.*, 2013, **13**, 1776–1781.
- 20 X. Zhang, C. Xie, J. Jie, X. Zhang, Y. Wu and W. Zhang, *J. Mater. Chem. A*, 2013, **1**, 6593–6601.
- 21 O. Lopez-Sanchez, E. Alarcon Llado, V. Koman, F. I. M. Anna, A. Radenovic and A. Kis, *ACS Nano*, 2014, **8**, 3042.
- 22 R. Cheng, D. Li, H. Zhou, C. Wang, A. Yin, S. Jiang, Y. Liu, Y. Chen, Y. Huang and X. Duan, *Nano Lett.*, 2014, **14**, 5590–5597.
- 23 F. Withers, P. O. Del, A. Mishchenko, A. P. Rooney, A. Gholinia, K. Watanabe, T. Taniguchi, S. J. Haigh, A. K. Geim and A. I. Tartakovskii, *Nat. Mater.*, 2015, **14**, 301.
- 24 W. J. Yu, Z. Li, H. Zhou, Y. Chen, Y. Wang, Y. Huang and X. Duan, *Nat. Mater.*, 2013, **12**, 246–252.
- 25 H. Yang, J. Heo, S. Park, H. J. Song, D. H. Seo, K. E. Byun, P. Kim, I. Yoo, H. J. Chung and K. Kim, *Science*, 2012, **336**, 1140.
- 26 C. Ojedaaristizabal, W. Bao and M. S. Fuhrer, *Phys. Rev. B: Condens. Matter Mater. Phys.*, 2013, **88**, 2466–2472.
- 27 A. Chen, H. Zhu, Y. Wu, G. Lou, Y. Liang, J. Li, Z. Chen, Y. Ren, X. Gui, S. Wang and Z. Tang, *ACS Photonics*, 2017, **4**, 1286–1291.
- 28 D. Vanmaekelbergh and L. K. van Vugt, *Nanoscale*, 2011, **3**, 2783–2800.
- 29 S. Chu, G. Wang, W. Zhou, Y. Lin, L. Chernyak, J. Zhao, J. Kong, L. Li, J. Ren and J. Liu, *Nat. Nanotechnol.*, 2011, **6**, 506–510.
- 30 R. Bao, C. Wang, L. Dong, C. Shen, K. Zhao and C. Pan, *Nanoscale*, 2016, **8**, 8078–8082.
- 31 C. X. Shan, J. S. Liu, Y. J. Lu, B. H. Li, F. C. Ling and D. Z. Shen, *Opt. Lett.*, 2015, **40**, 3041–3044.
- 32 Y. J. Lu, Z. F. Shi, C. X. Shan and D. Z. Shen, *Chin. Phys. B*, 2017, **26**, 50–58.
- 33 X. Yang, C. X. Shan, Y. J. Lu, X. H. Xie, B. H. Li, S. P. Wang, M. M. Jiang and D. Z. Shen, *Opt. Lett.*, 2016, **41**, 685.
- 34 Z. F. Shi, T. T. Xu, D. Wu, Y. T. Zhang, B. L. Zhang, Y. T. Tian, X. J. Li and G. T. Du, *Nanoscale*, 2015, **8**, 9997.
- 35 P. N. Ni, C. X. Shan, S. P. Wang, Y. J. Lu, B. H. Li and D. Z. Shen, *Appl. Phys. Lett.*, 2015, **107**, 2278.
- 36 B. Wu, S. W. Zhuang, C. Chi, Z. F. Shi, J. Y. Jiang, X. W. Chu, X. Dong, W. C. Li, G. X. Li and Y. T. Zhang, *Semicond. Sci. Technol.*, 2016, **31**, 035012.
- 37 X. Ji, A. Wang, G. Li and Z. Lu, *Micro Nano Lett.*, 2016, **11**, 753–757.
- 38 X. Yang, L. Dong, C. Shan, J. Sun, N. Zhang, S. Wang, M. Jiang, B. Li, X. Xie and D. Shen, *Adv. Mater.*, 2017, **29**, 1602832.
- 39 M. H. Huang, S. Mao, H. Feick, H. Yan, Y. Wu, H. Kind, E. Weber, R. Russo and P. Yang, *Science*, 2001, **292**, 1897–1899.
- 40 F. Li, L. Orosz, O. Kamoun, S. Bouchoule, C. Brimont, P. Disseix, T. Guillet, X. Lafosse, M. Leroux and J. Leymarie, *Phys. Rev. Lett.*, 2013, **110**, 196406.
- 41 H. Zhu, C. X. Shan, B. Yao, B. H. Li, J. Y. Zhang, Z. Z. Zhang, D. X. Zhao, D. Z. Shen, X. W. Fan and Y. M. Lu, *Adv. Mater.*, 2009, **21**, 1613–1617.
- 42 C. Xu, J. Dai, G. Zhu, G. Zhu, Y. Lin, J. Li and Z. Shi, *Laser Photonics Rev.*, 2014, **8**, 469–494.
- 43 J. Dai, C. X. Xu, P. Wu, J. Y. Guo, Z. H. Li and Z. L. Shi, *Appl. Phys. Lett.*, 2010, **97**, 1221.
- 44 J. Dai, C. X. Xu and X. W. Sun, *Adv. Mater.*, 2011, **23**, 4115.